Electroluminescence from Serpentine Carbon Nanotube Based Light-Emitting Diodes on Quartz

Dangmin Yu, Sheng Wang, Linhui Ye, Wei Li, Zhiyong Zhang, Yabin Chen, Jin Zhang, and Lian-Mao Peng**

Semiconducting single-walled carbon nanotubes (SWCNTs), with their direct bandgap and one-dimensional (1D) structure, have promising applications in nanoelectronics and optoelectronic devices,[1,2] including in carbon-nanotube (CNT)-based near-infrared light sources, as saturable absorbers in ultrafast lasers,[3] as infrared detectors in optical communication, in photovoltaic cells,[4] as quantum light sources,[5] and in fluorescent biolabeling.[6] In particular, CNT-based light sources, including those based on field-effect transistors (FETs) and light-emitting diodes (LEDs), have been made using both single SWCNTs and thin films of them.[7–15] The basic electroluminescence (EL) mechanism and properties of single-CNT-based light sources have been investigated. However, due to the low current capability of a single CNT, these devices usually have relatively low EL intensity and poor homogeneity in device performance, which limits the applications of these single-nanotube emitters. To overcome these limitations, thin-film emitting devices were fabricated using both network and aligned arrays of CNTs which can sustain much larger current than devices based on individual CNTs. However, emission peaks in EL spectra obtained from these CNT-film-based devices are very broad and are also dependent on the nanotube-diameter distribution, and the EL processes are further complicated due to the exciton transfer from small-diameter CNTs to larger ones.[16,17] Furthermore, the presence of metallic CNTs in these films leads to a low emission efficiency due to the quenching process of excitons with nonradiative energy transfer.[13,18] In an early report, near single-chirality CNT-array FETs were fabricated by using purified CNT samples obtained by density gradient ultracentrifugation.[19] However, the device performance was severely limited by the poor material quality of the solution-treated CNTs, in which large quantity of defects were present. Here we report the fabrication and performance characteristics of light-emitting devices that use serpentine CNTs grown directly on quartz. These serpentine-CNT-based light-emitting devices have multiple parallel CNT channels of identical chirality; this represents the ideal structure for scaling up the power of the CNT LEDs, which are free of the usual negative effects that are due to the complicated interactions between CNTs of different diameters and chiralities. EL results obtained from the serpentine-CNT-based LEDs are compared with that from a device based on a single CNT on SiO_2/Si and on aligned arrays of CNTs on quartz, which makes it possible to analyze the EL mechanism of the CNT LED devices and to integrate these highly efficient emitting devices with other optoelectronic components, such as photodetectors, in on-chip optical interconnect systems.[20]

Serpentine CNTs were grown on quartz by using a chemical vapor deposition (CVD) method, as previously reported.[21–23] One striking feature relevant to this work is that the serpentine CNT has many parallel CNT segments with identical chirality (**Figure 1**a). This complex CNT morphology is a result of several factors that compete with each other during the growth process, in particular the gas flow and the strong interaction between nanotube and substrate lattice.[21–23] Two-terminal device geometry with asymmetric metal contacts is used in this work. Briefly, the serpentine-CNT-based LED was fabricated directly on quartz substrate by using palladium as the hole or p contact and scandium as the electron or n contact. Earlier studies shown that Sc or Y can form a perfect ohmic contact with the conduction band of the CNTs,[24,25] while Pd can form a perfect ohmic contact with the valence band of the CNTs.[26] A semiconducting CNT asymmetrically contacted by these two types of contacts acts effectively as a p–n junction with high carrier-injection efficiency and low operating voltage.[27] This doping-free method may readily be adopted to fabricate highly efficient LEDs by using serpentine CNTs to create many parallel CNT channels of identical chirality in each LED device. Since the EL intensity from a CNT LED is directly proportional to the device current, the use of serpentine CNTs is highly beneficial. A single CNT channel can typically sustain a few microamperes of current, while greater than 25 μA may generate more heat in the CNT than that would be effectively dissipated, which leads to electric breakdown of

D. M. Yu, Dr. S. Wang, L. H. Ye, W. Li, Dr. Z. Y. Zhang, Prof. L.-M. Peng
Key Laboratory for the Physics and Chemistry of Nanodevices
Department of Electronics
Peking University
Beijing, 100871, China
E-mail: shengwang@pku.edu.cn; lmpeng@pku.edu.cn
Y. B. Chen, Prof. J. Zhang
College of Chemistry and Molecular Engineering
Peking University
Beijing, 100871, China

DOI: 10.1002/smll.201302287

 © 2013 Wiley-VCH Verlag GmbH & Co. KGaA, Weinheim

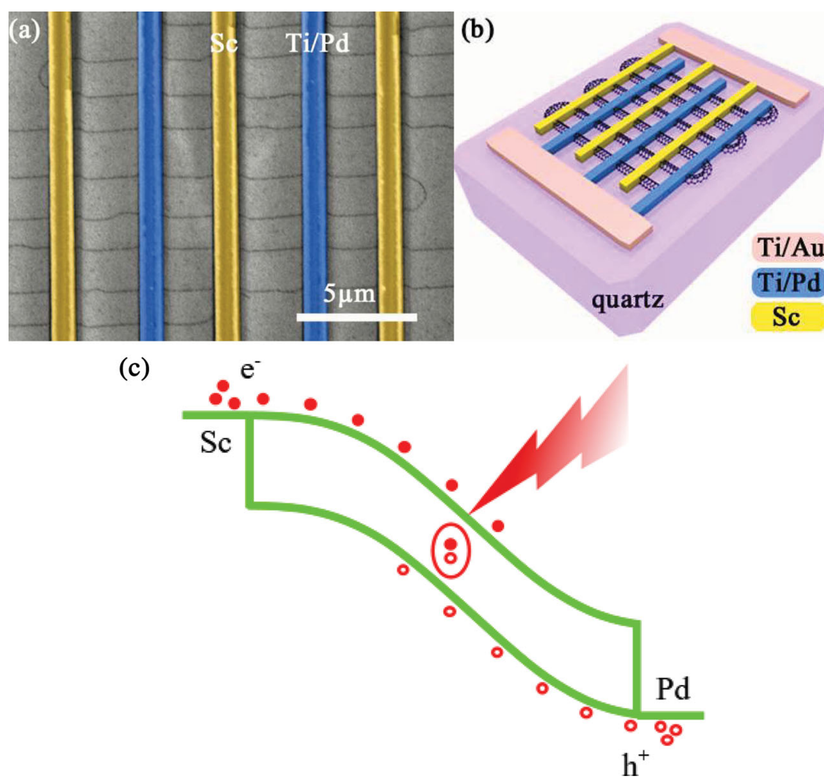

Figure 1. Structure and operation principle of CNT LED arrays. a) SEM image showing serpentine-CNT-based diode arrays on quartz. The CNT is grown by CVD, and is contacted asymmetrically by Sc (70 nm, yellow) and Ti/Pd (0.3/70 nm, blue). The width of the contact is about 0.5 μm and the channel length is about 2 μm. b) Schematic of device structure of the CNT LED arrays fabricated using asymmetric contacts on quartz substrate. In addition to the Sc and Ti/Pd contacts, test pads are also connected to these contacts; in real devices these are made of Ti/Au. c) Schematic energy-band diagram showing a CNT diode at high forward bias. Electrons and holes are injected into the channel from Sc and Ti/Pd electrodes, respectively.

the CNT channel. Typically a serpentine CNT can provide ten parallel channels for the current, which leads to a current capability of about a few tens of microamperes, and this current level can be further increased to milliampere level by using a finger structure as shown in Figure 1b. To protect and improve the stability of the device, the device is fully covered with a 180-nm thin film of polymethylmethacrylate (PMMA). Details of the device fabrication and EL measurements can be found in the Experimental Section.

Conventionally, CNT light-emitting devices can be divided into two types: 1) Ambipolar type, where electrons and holes are injected into the channels simultaneously and form excitons which subsequently recombine to yield EL; examples of this type of devices including ambipolar FETs,[1–8] p-i-n diodes based on split-gate FETs,[7] and two-terminal LED with asymmetric metal contacts.[4,9] 2) Unipolar type, where only one type of carrier (electrons or holes) is injected into the channel, and the excitons are created locally through such effects as impact ionization and then recombine radiatively.[1,14] Figure 1c is a schematic illustration of EL mechanism of the two-terminal CNT LED with asymmetric Sc and Pd contacts. At high forward bias, electrons and holes are injected into the CNT channel without barrier, and some of them will form excitons via Coloumb interaction and subsequently recombine to yield infrared emission. At zero or low reverse bias, both types of carriers (electrons and holes) are subjected to a large potential barrier (of the order of the bandgap of the CNT), and the device current is significantly reduced from that at forward bias.[4,9]

Figures 2a and 2b show two typical current–voltage (*I–V*) plots of two serpentine-CNT-based devices on quartz, which may be readily used for identifying the electric properties of the serpentine CNT, i.e., whether it is metallic or semiconducting. For a semiconducting serpentine-CNT-based device, the *I–V* curve exhibits a typical rectifying-diode behavior (Figure 2a). On the other hand, for a metallic serpentine-CNT-based device, the *I–V* curve appears symmetric with typical linear behavior at low bias that changes to saturation behavior at high bias with V = 2 V (Figure 2b). This change arises because a metallic CNT can form ohmic contact with both Pd and Sc contacts. To further verify these results, a top-gate FET with a 45-nm Al_2O_3 dielectric and 10-nm Pd metal gate was fabricated after EL measurements and the device (that shown in Figure 2a) showed a current on–off ratio of more than 100 (Figure 2c), which is characteristic of a semiconducting CNT. The asymmetric-contact method is convenient to identify CNT properties without needing to ascertain transfer characteristics of the device, which can only be measured through additional gate-voltage control, as in FET devices. This method is especially convenient for identifying CNTs grown on such substrates as quartz and polymer, since these materials are insulating and cannot be used as back gates, as in the case of SiO_2/Si substrates.

Since effectively tens of identical CNT channels are involved in our serpentine-CNT-based LED with finger structure (Figure 1b), the total current in the device is significantly larger than that in a device based on a single CNT, and leads to much stronger EL intensity. Figure 2d shows a typical infrared emission spectrum obtained from a semiconducting serpentine-CNT-based LED measured with a bias V = 3.2 V and current I = 52 μA. Two emission peaks can be identified. The lower energy emission peak (peak 1) is at 0.85 eV with a full width at half-maximum (FWHM) value of 42 meV, and the higher energy peak (peak 2) is at 0.94 eV with a wider FWHM of 124 meV. To identify the nature of these emission peaks, we characterized the CNT by atomic force microscopy (AFM), and the diameter of the nanotube is estimated to be 1.1 ± 0.2 nm (Supporting Information, Figure S1). A semiconducting CNT with this diameter is associated with a photoluminescence (PL) peak due to the E_{11} exciton transition at about 0.85 eV,[28] which is the same energy as peak 1 of Figure 2d. The FWHM of this EL peak is also in the same

© 2013 Wiley-VCH Verlag GmbH & Co. KGaA, Weinheim

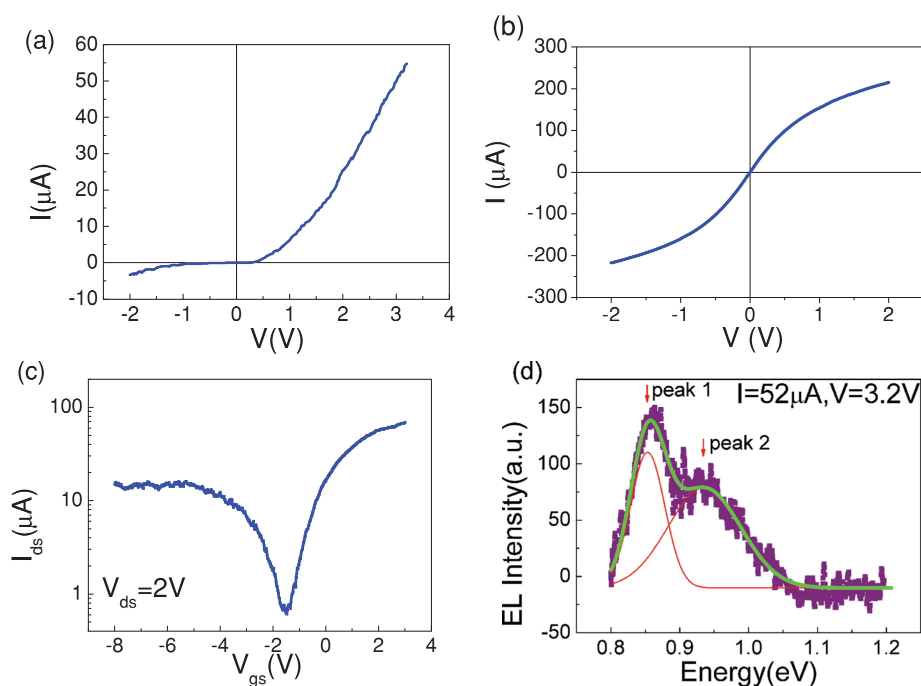

Figure 2. Electric and EL characteristics of serpentine-CNT-based diode arrays. a) Typical experimental *I–V* characteristic of an asymmetrically contacted serpentine-CNT-diode device. The channel length was about 2 μm. b) *I–V* characteristic of a metallic serpentine CNT contacted by asymmetric Pd/Sc contacts. c) Transfer characteristic of the device used in (a). The drain–source voltage was 2 V, and the transfer characteristics were obtained by scanning the top-gate source voltage from −8 to 3 V. d) A typical EL spectrum obtained from the CNT-diode-array device. This spectrum can be fitted by using two Gaussian functions (red lines) that peak at 0.85 and 0.94 eV, with FWHM values of 42 and 124 meV for the two peaks, respectively. The green line denotes the sum of the two fitting Gaussian functions.

order of magnitude as that of the room temperature PL and EL spectra with asymmetric contacts or electrostatically doped p-i-n diodes, i.e., about 25 to 40 meV.[29–31] The lower energy emission peak (peak 1) can thus be identified as coming from the E_{11} excitonic transition of the CNT and the higher energy peak (peak 2) with a FWHM 124 meV is obviously different from the single-chirality CNT EL results on SiO_2/Si substrate. The FWHM of peak 2 is much wider than that of peak 1, which is typical of an excitonic E_{11} transition of the CNT. Peak 2 also cannot be identified as the E_{11} continuum. The exciton binding energy (E_b) for a CNT with $d = 1.1$ nm and embedded in SiO_2/PMMA dielectric is about 0.2–0.3 eV. This large value is due to the 1D structure of the CNT and the less-effective dielectric screening in this environment, which is SiO_2 (with $\varepsilon_{eff} \approx 2.5$) covered with PMMA (with $\varepsilon_{eff} \approx 3$). So the bandgap of the CNT is estimated to be about 1.05–1.15 eV, which is much larger than the corresponding energy value of peak 2 at 0.94 eV. The emission peak 2 is thus excluded from coming from the interband transition.[32] It should be noted that in our devices the operating voltage (ca. 2–3 V) is relatively low, and this low bias cannot provide a sufficiently strong local electric field to arouse the strong interaction of the excitonic state E_{11} with higher energy excitonic or band-to-band continuous states.[1,7] At the same time, the lineshape of the interband transition peak is usually not symmetric because of the mixture of the excitonic states and the continuum states. However, peak 2 at 0.94 eV appears clearly at low voltage with a symmetric lineshape (Figure 2d), and cannot thus be identified as the E_{11} continuum. Another possibility for the appearance of this peak is the blackbody radiation caused by Joule heating. We can estimate the temperature of the carbon nanotube by using the measured energy value for peak 2 (0.94 eV) and Wien displacement law to yield Equation (1)

$$T = \frac{b}{\lambda_{max}} = \frac{2.90 \times 10^6}{1240/0.94} \mathrm{K} \approx 2.34 \times 10^3 \mathrm{K}, \quad (1)$$

i.e., if a CNT is going to produce an energy peak at 0.94 eV as for peak 2 in Figure 2d via blackbody radiation, the temperature of the CNT would be 2340 K. However, it is impossible for a device fabricated on quartz to reach such a high temperature, because quartz has a large thermal conductivity, and is very effective at releasing heat generated by the device. On the other hand, serpentine CNTs grown on quartz have strong interactions with the substrate, and previous reports have proved that the interaction between nanotube and quartz leads to an obvious "up-shift" of the G-band frequencies of aligned SWCNTs that originates from the C–C deformation.[33,34] We thus propose that this high-energy peak at 0.94 eV comes from a new exciton state caused by strong periodic interaction between the CNTs and the quartz substrate.[35] A similar peak has also been observed in EL spectra obtained from other CNT devices on quartz, see Figure S2a. To further verify the interaction between the CNT and quartz substrate, Raman spectra were obtained from the serpentine-CNT device with the structure illustrated in Figure S2b. The serpentine CNT may be roughly

© 2013 Wiley-VCH Verlag GmbH & Co. KGaA, Weinheim

divided into two types of segement, i.e., A-type CNT that is aligned along the surface steps of the quartz substrate and B-type CNT that crosses the step. The G and G' band of both segments A and B are shown as Figures S2c–f. When the CNT (segment A) is parallel to the surface step, the G band is broadened and four peaks appear at 1554.9, 1567.9, 1578.2, and 1593.8 cm^{-1} (Figure S2c), showing a complicated structure that is the same as reported in reference 34. When the CNT (segment B) crosses the surface step, the G band shows typical semiconductor characteristics (Figure S2d) and the G^- and G^+ peaks appear at 1589.9 and 1595.8 cm^{-1}, respectively. Furthermore, the G' band of segment A is split into two peaks at 2648.6 and 2666.8 cm^{-1} due to the strong interaction between the CNT and substrate, which is also consistent with the results reported in reference [34]. The G' band of segment B only exhibits a peak at 2647.2 cm^{-1}. We thus conclude that the characteristics of the G and G' bands of segment A are caused by the strong interaction between the serpentine CNT and quartz substrate, which indicates that the new exciton observed in our experiment is due to periodic modulation caused by the CNT–substrate interaction.

To compare the performance of serpentine-CNT-based devices with those based on single CNTs on SiO_2/Si, a similar finger-structure device was fabricated on an ultralong SWCNT as illustrated in **Figure 3**a. Three pairs of parallel Pd and Sc contacts were deposited on a single semiconducting CNT to multiply the current and thus EL intensity of the CNT LED. The transfer behavior of the single-CNT-based device exhibits typically ambipolar behavior (Figure 3b) which is similar to that shown in Figure 2c for the serpentine-CNT-based device. At a back-gate voltage V_{gs} = 4 V, the device is in its OFF state and the corresponding *I–V* characteristic (Figure 3c) shows typical diode-rectifying behavior and a large current of about 80 μA at forward voltage V = 2V. EL spectra were obtained at V_{gs} = 4 V, and the two spectra shown in Figure 3d correspond to I_{ds} = 80 and 90 μA. Unlike those obtained from the serpentine-CNT-based devices on quartz, the spectra obtained from a single-CNT-based device on SiO_2/Si can be fitted with a single Gauss–Lorentz peak. The peak position is at 1.03 eV for both spectra, and the FWHM is about 76 and 77 meV for the two spectra. We also characterized the CNT by Raman spectroscopy with 632.8-nm laser excitation (Figure S3). The radial breathing mode (RBM) peak is at $\Omega \approx 227$ cm^{-1}, which yields a diameter for the CNT $d = 248/\Omega \approx 1.09$ nm and which corresponds well to the EL spectral peak energy at 1.03 eV. The narrow FWHM in Figure 3d suggests that the EL peak comes from the E_{11} exciton. The inset of Figure 3d shows that the EL integrated intensity varies linearly with the current passing through the CNT channels for both the device based on a single CNT on SiO_2/Si and that based on a serpentine CNT on quartz. Since the single ultralong CNT on SiO_2/Si is a quasi-1D system, the emitting spots are restricted to a 1D line instead of a 2D plane as in the serpentine CNT case. Because it is restricted by the finite numerical aperture of the lens in our measurement system, the total number of parallel diodes that can be detected is limited and a relatively large operating current or voltage is needed to obtain enough counts in the detector. This fact means that a greater current is required in each constituent CNT channel in the single-CNT-based device than in that based on the serpentine CNT to achieve the same integrated intensity. However, since the upper current value must be less than 25 μA for each CNT channel to avoid possible electric breakdown resulting from Joule heating, it is difficult to obtain the same integrated intensity level in a single-CNT-based device as that in the serpentine-CNT-based device. The slope of the integrated EL intensity vs. current curve in the inset of Figure 3d may be considered to be related to the number of photons excited by unit of carriers, and is related to the efficiency of the light-emitting device. From the inset of Figure 3d, we can see that the slope of the serpentine-CNT-based LED on quartz is slightly smaller than that of the device based on a single CNT on SiO_2/Si, which suggests that the efficiency of the serpentine-CNT-based LED on quartz is comparable to but smaller than that based on a single CNT on silicon oxide. This result is because CNTs can interact strongly with

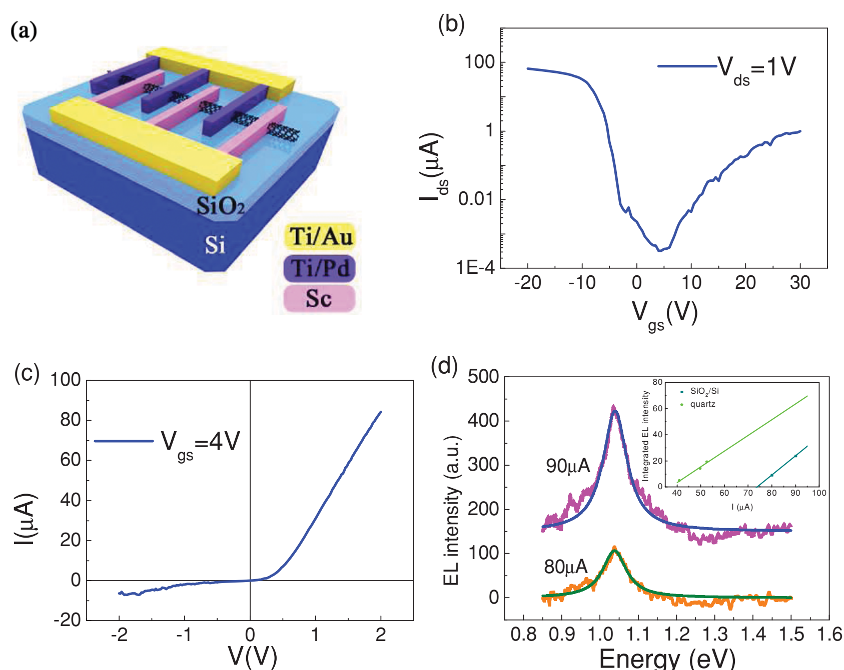

Figure 3. Electric and EL characteristics of diodes based on a single CNT on SiO_2/Si. a) Device structure diagram showing a single-CNT-based LED device with asymmetric contacts. The parallel finger contact structure is utilized to increase the total device current. The channel length is about 2 μm and the substrate is 500 nm thick SiO_2 on n++ Si. b) Transfer characteristics of the single-CNT-based diode at V_{ds} = 1 V; the back-gate voltage was scanned from −20 to 30 V. c) *I–V* behavior of the device at V_{gs} = 4 V. d) EL spectra of the device on SiO_2/Si substrate. The inset shows the integrated EL intensity plots as a function of device current for the serpentine-CNT-based LEDs on quartz and SiO_2/Si.

© 2013 Wiley-VCH Verlag GmbH & Co. KGaA, Weinheim

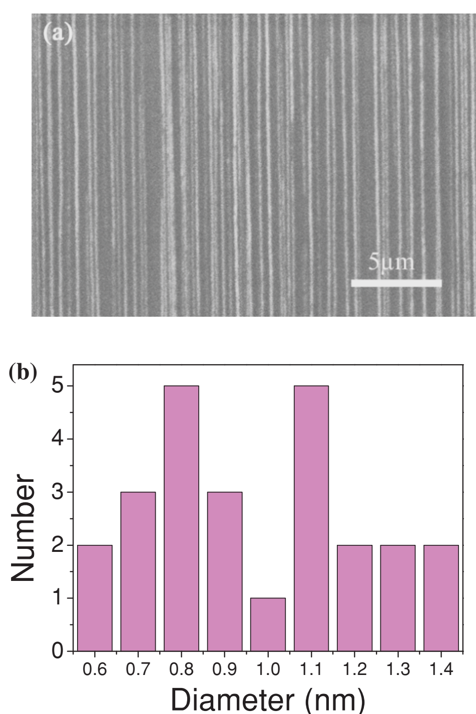

Figure 4. Characteristics of aligned-CNT arrays on quartz. a) SEM image showing a CNT film composed of parallel arrays of CNTs. b) Diameter distribution of the CNT aligned arrays. The overall distribution of the tube diameters corresponds to an energy gap range from 0.8–1.55 eV for semiconducting CNTs.

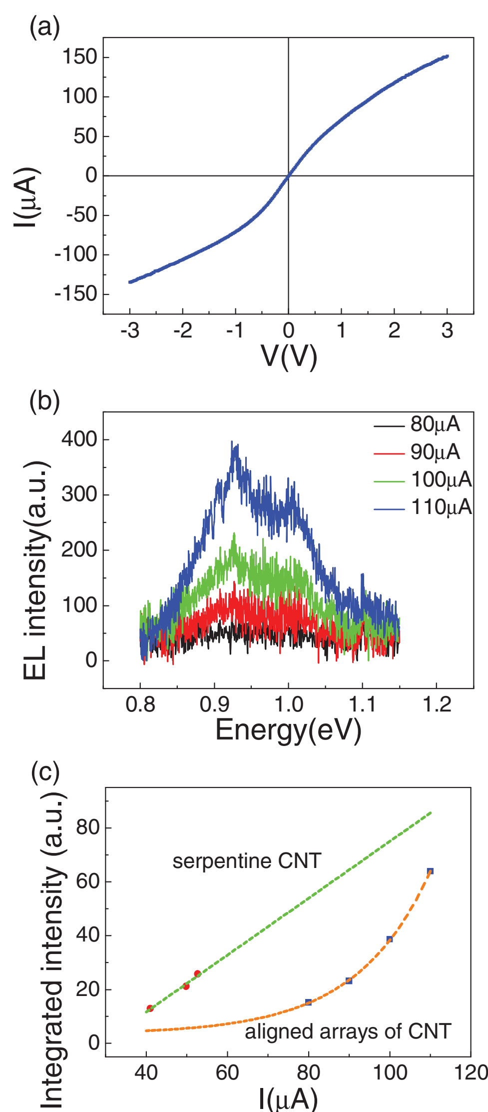

Figure 5. Electric and EL characteristics of CNT diodes based on aligned arrays and comparison with that based on serpentine CNT on quartz. a) *I–V* characteristic of a CNT aligned array based diode with asymmetric contacts. b) EL spectra of the device at different currents. c) Integrated EL intensity as a function of device current for serpentine-CNT and CNT array film based diodes.

quartz substrate which may lead to enhanced nonradiative exciton recombination. We expect that the efficiency of the serpentine-CNT-based LED may be further improved by transferring serpentine CNTs to other substrates which have little interaction with the CNTs, such as SiO_2/Si and organic materials.

To compare the EL properties of the serpentine-CNT-based LED with that based on aligned arrays of CNT on quartz, we investigated the EL emission of a CNT array film based device with a similar device structure. Aligned arrays of CNTs were prepared on quartz by CVD (**Figure 4**a) and devices were fabricated by using the same asymmetric Pd–Sc contacts. The statistical distribution of the nanotube diameters in our test sample is shown in Figure 4b. Since the diameter distribution is relatively narrow (0.6–1.4 nm), the detector can detect most EL signals from CNTs with energy ranging from ca. 0.8–1.55 eV. A typical *I–V* curve measured from these devices is shown in **Figure 5**a. At low bias, the *I–V* is basically linear, which suggests metallic behavior, but the current tends to saturate at high bias toward different levels, with the current being 152 μA at 3 V and –134 μA at –3 V. This peculiar *I–V* characteristic is due to the fact that the CNT-array film is composed of mixed metallic and semiconducting CNTs. At low bias, metallic CNTs dominate the transport and current increases linearly with bias. At high bias, both metallic and semiconducting CNTs contribute to the total current. Scattering, especially that by optical phonons, begins to play an important role, leading to current saturation at high bias. Since the CNTs are contacted by asymmetric metals with excellent contacts to the conduction and valence bands of semiconducting CNTs, at high forward bias both electrons and holes may be injected into the CNTs with high efficiency and contribute to the total current (Figure 1c). At reverse bias, the situation is different. Both electrons and holes are subjected to a potential barrier which severely limits the contributions from semiconducting CNTs with small diameter or large bandgap, resulting in a smaller total device current at high negative bias than that at high forward bias.

While the *I–V* characteristic of the CNT array film based device is dominated by metallic CNTs at low bias, the metallic CNTs on a substrate with good thermal conductance may contribute to EL only at very large electric field, and the EL spectra collected from the CNT array film based LED

© 2013 Wiley-VCH Verlag GmbH & Co. KGaA, Weinheim

(Figure 5b) are dominated by semiconducting CNTs at low bias. By comparing the spectra with that shown in Figure 2d for the serpentine-CNT-based device, it is clear that the spectra obtained from the aligned CNT arrays are more complex with many broad features. This complexity is caused by the presence of CNTs of different diameters and chiralities in the CNT arrays film; each contributes an emission peak of different energy. Unlike the serpentine-CNT-based LED, in which the emission channels are identical and the integrated EL intensity increases linearly with the current, the integrated EL intensity for the CNT array film based device varies with the current nonlinearly, and may be fitted to a good approximation by an exponential as shown in Figure 5c. At low bias or current, the EL intensity is much lower than that from the serpentine-CNT-based LED, because much of the current is conducted in the metallic CNTs which hardly contribute to the detected EL intensity. At high bias or current, metallic CNTs begin to saturate and the current of semiconducting CNTs account for a greater proportion of the EL signal, which leads to a significant enhancement of the EL intensity. Another reason for the nonlinear relationship is that the diameters of the CNTs are smaller than those of single CNTs and serpentine CNTs, so there may be a small barrier between the CNTs and the contacts in the forward situation for such small-diameter CNTs. The ambipolar and unipolar EL can coexist, which leads to an exponential relation of EL intensity and current. However, at high bias other effects also begin to affect the device performance, such as electric breakdown, exciton–exciton annihilation,[36] and higher-order excitations, which may lead to new restricting factors.

In summary, we investigated the EL characteristics of serpentine carbon nanotube based LEDs on a quartz substrate. The serpentine CNT provides multiple conduction channels of single chirality for the device, without introducing complex junctions and excitons transfer between nanotubes as in thin-film devices. The device was fabricated on the serpentine CNT simply by contacting the CNT with two asymmetric contacts which may connect directly to the conduction (Sc contact) and valence (Pd contact) bands of the CNT. The emission intensity of the device increases linearly with current so that we can adjust the intensity easily by tuning the voltage or the current. We also compared the performance of the serpentine-CNT-based device with those based on single-CNT LEDs on SiO_2/Si substrate and aligned arrays of CNT devices on quartz. The LEDs based on serpentine CNTs are shown to outperform the others due to the larger device current, higher emission intensity, and narrower emission bands which are important for real optoelectronic applications of nanoscale light sources.

Experimental Section

Sample Preparation: Three different types of CNT were used in this work. 1) Serpentine carbon nanotubes were prepared by CVD on st-cut quartz.[21] The carbon nanotubes are composed of repeated parallel segments which have the same chirality. 2) Ultra-long individual SWCNTs were prepared by CVD on SiO_2/Si, with a SiO_2 thickness of about 500 nm. 3) Aligned parallel CNT array films were prepared by CVD on quartz.

The electrodes of diode devices were patterned by using electron-beam lithography (EBL) and a lift-off process. A film of water-soluble conducting polymer (Espacer 300Z, Showa Denko K. K.) was applied on top of the PMMA to prevent charging of PMMA during the EBL on quartz. Asymmetric Sc and Ti/Pd electrodes were deposited on CNTs (Figures 1b and 3a) via e-beam evaporation under high vacuum. The thickness of the Sc and Ti/Pd contacts was 70 and 0.3/70 nm, respectively. A small amount of Ti was used to increase the adhesion between the Pd and the quartz substrate, and has little influence on the p-type contact. The test pad was made of 5/45-nm Ti/Au. Typically, the device was fully covered with an about 180-nm thin film of PMMA to improve its stability. The channel length of the device is 2 µm.

Measurements: Electrical measurements were carried out with a Keithley 4200 semiconductor analyzer at room temperature. EL measurements were carried out with a 150 line/mm grating and a liquid-nitrogen-cooled InGaAs detector linear array of 512×1 pixels (detects $E > 0.8$ eV) (JobinYvon/Horiba company) and collected using a microscope objective (50×) lens. The typical integration time for collecting an EL spectrum was 90 s. All measurements were performed in air.

Supporting Information

Supporting Information is available from the Wiley Online Library or from the author.

Acknowledgements

This work was supported by the Ministry of Science and Technology (Grant Nos. 2011CB933002 and 2011CB933001), National Science Foundation of China (Grant Nos. 61271051, 61321001, 61370009 and 10974002), and Beijing Municipal Science and Technology Commission (Z121100001312003).

[1] P. Avouris, M. Freitag, V. Perebeinos, *Nat. Photonics* **2008**, *2*, 341–350.
[2] L. J. Carlson, T. D. Krauss, *Acc. Chem. Res.* **2008**, *41*, 235–243.
[3] A. G. Rozhin, Y. Sakakibara, S. Namiki, M. Tokumoto, H. Kataura, Y. Achiba, *Appl. Phys. Lett.* **2006**, *88*, 051118.
[4] L. J. Yang, S. Wang, Q. S. Zeng, Z. Y. Zhang, T. Pei, Y. Li, L.-M. Peng, *Nat. Photonics* **2011**, *5*, 672–676.
[5] A. Hogele, C. Galland, M. Winger, A. Imamoglu, *Phys. Rev. Lett* **2008**, *100*, 217401.
[6] T. K. Leeuw, R. M. Reith, R. Simonette, M. E. Harden, P. Cherukuri, D. A. Tsyboulski, K. M. Beckingham, R. B. Weisman, *Nano Lett.* **2007**, *7*, 2650–2654.
[7] T. Mueller, M. Kinoshita, M. Steiner, V. Perebeinos, A. A. Bol, D. B. Farmer, P. Avouris, *Nat. Nanotechnol.* **2010**, *5*, 27–31.
[8] J. A. Misewich, R. Martel, P. Avouris, J. C. Tsang, S. Heinze, J. Tersoff, *Science* **2003**, *300*, 783–786.
[9] S. Wang, Q. S. Zeng, L. J. Yang, Z. Y. Zhang, Z. X. Wang, T. Pei, L. Ding, X. L. Liang, M. Gao, Y. Li, L. M. Peng, *Nano Lett.* **2011**, *11*, 23–29.

© 2013 Wiley-VCH Verlag GmbH & Co. KGaA, Weinheim

[10] M. H. P. Pfeiffer, N. Stürzl, C. W. Marquardt, M. Engel, S. Dehm, F. Hennrich, M. M. Kappes, U. Lemmer, R. Kurpke, *Opt. Express* **2011**, *19*, A1184–A1189.
[11] N. Hibino, S. Suzuki, H. Wakahara, Y. Kobayashi, T. Sato, H. Maki, *ACS Nano* **2011**, *5*, 1215–1222.
[12] M. Freitag, V. Perebeinos, J. Chen, A. Stein, J. C. Tsang, J. A. Misewich, R. Martel, P. Avouris, *Nano Lett.* **2004**, *4*, 1063–1066.
[13] M. Kinoshita, M. Steiner, M. Engel, J. P. Small, A. A. Green, M. C. Hersam, R. Krupke, E. E. Mendez, P. Avouris, *Opt. Express* **2010**, *18*, 25738–25745.
[14] J. Zaumseil, X. N. Ho, J. R. Guest, G. P. Wlederrecht, J. A. Rogers, *ACS Nano* **2009**, *3*, 2225–2234.
[15] X. Xie, A. E. Islam, M. A. Wahab, L. Ye, X. Ho, M. Alam, J. A. Rogers, *ACS Nano* **2012**, *6*, 7981–7988.
[16] D. Y. Joh, J. Kinder, L. H. Herman, S.-Y. Ju, M. A. Segal, J. N. Johnson, G. K.-L. Chan, J. Park, *Nat. Nanotechnol.* **2011**, *6*, 51–56.
[17] M. Engel, J. P. Small, M. Steiner, M. Freitag, A. A. Green, M. C. Hersam, P. Avouris, *ACS Nano* **2008**, *2*, 12.
[18] E. Adam, C. M. Aguirre, L. Marty, B. C. St-Antoine, F. Meunier, P. Desjardins, D. Ménard, R. Martel, *Nano Lett.* **2008**, *8*, 2351–2355.
[19] A. Vijayaraghavan, F. Hennrich, N. Sturzl, M. Engel, M. Ganzhorn, M. Oron-Carl, C. W. Marquardt, S. Dehm, S. Lebedkin, M. M. Kappes, R. Krupke, *ACS Nano* **2010**, *4*, 2748–2754.
[20] A. Nojeh, A. Ivanov, *IEEE Design and Test of Computers* **2010**, *27*, 44–52.
[21] Y. G. Yao, X. C. Dai, C. Q. Feng, J. Zhang, X. L. Liang, L. Ding, W. Choi, J. Y. Choi, J. M. Kim, Z. F. Liu, *Adv. Mater.* **2009**, *21*, 4158–4162.
[22] S. Jeon, C. Lee, J. Tang, J. Hone, C. Nuckolls, *Nano Res.* **2008**, *1*, 427–433.
[23] N. Geblinger, A. Ismach, E. Joselevich, *Nat. Nanotechnol.* **2008**, *3*, 195–200.
[24] Z. Y. Zhang, X. L. Liang, S. Wang, K. Yao, Y. F. Hu, Y. Z. Zhu, Q. Chen, W. W. Zhou, Y. Li, Y. G. Yao, J. Zhang, L. M. Peng, *Nano Lett.* **2007**, *7*, 3603–3607.
[25] L. Ding, S. Wang, Z. Y. Zhang, Q. S. Zeng, Z. X. Wang, T. Pei, L. J. Yang, X. L. Liang, J. Shen, Q. Chen, R. L. Cui, Y. Li, L. M. Peng, *Nano Lett.* **2009**, *9*, 4209–4214.
[26] A. Javey, J. Guo, Q. Wang, M. Lundstrom, H. J. Dai, *Nature* **2003**, *424*, 654–657.
[27] S. Wang, Z. Y. Zhang, L. Ding, X. L. Liang, J. Sun, H. L. Xu, Q. Chen, R. L. Cui, Y. Li, L. M. Peng, *Adv. Mater.* **2008**, *20*, 3258–3262.
[28] R. B. Weisman, S. M. Bachilo, *Nano Lett.* **2003**, *3*, 1235–1238.
[29] S. M. Bachilo, M. S. Strano, C. Kittrell, R. H. Hauge, R. E. Smalley, R. B. Weisman, *Science* **2002**, *298*, 2361–2366.
[30] M. J. O' Connell, S. M. Bachilo, C. B. Huffman, V. C. Moore, M. S. Strano, E. H. Haroz, K. L. Rialon, P. J. Boul, W. H. Noon, C. Kittrell, J. Ma, R. H. Hauge, R. B. Weisman, R. E. Smalley, *Science* **2002**, *297*, 593–596.
[31] F. Wang, G. Dukovic, L. E. Brus, T. F. Heinz, *Science* **2005**, *308*, 838–841.
[32] G. Dukovic, F. Wang, D. H. Song, M. Y. Sfeir, T. F. Heinz, L. E. Brus, *Nano Lett.* **2005**, *5*, 2314–2318.
[33] L. Ding, W. W. Zhou, T. P. McNicholas, J. Y. Wang, H. B. Chu, Y. Li, J. Liu, *Nano Res.* **2009**, *2*, 903–910.
[34] J. S. Soares, A. P. M. Barboza, P. T. Araujo, N. M. B. Neto, D. Nakabayashi, N. Shadmi, T. S. Yarden, A. Ismach, N. Geblinger, E. Joselevich, C. Vilani, L. G. Cancado, L. Novotny, G. Dresselhaus, M. S. Dresselhaus, B. R. A. Neves, M. S. C. Mazzoni, A. Jorio, *Nano Lett.* **2010**, *10*, 5043–5048.
[35] L. H. Ye, D. M. Yu, S. Wang, Z. Y. Zhang, L.-M. Peng, unpublished.
[36] Y. Murakami, J. Kono, *Phys. Rev. Lett.* **2009**, *102*, 037401.

Received: July 26, 2013
Revised: September 29, 2013
Published online: November 8, 2013

© 2013 Wiley-VCH Verlag GmbH & Co. KGaA, Weinheim